NASA Technical Memorandum 78990

SPACECRAFT CHARGING CONTROL BY THERMAL, FIELD EMISSION WITH LANTHANUM-HEXABORIDE EMITTERS

James F. Morris
Lewis Research Center
Cleveland, Ohio 44135

August 1978

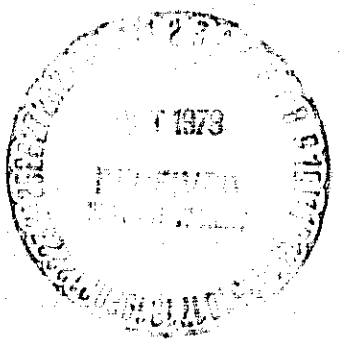

SPACECRAFT CHARGING CONTROL BY THERMAL, FIELD EMISSION WITH LANTHANUM-HEXABORIDE EMITTERS

by James F. Morris
NASA Lewis Research Center
Cleveland, Ohio

SUMMARY

Recently R. Grard (J. Geophys. Rsch., V. 81, No. 10 p. 1805, April 1976) elaborated on his concept of using cold tungsten field emitters for "spacecraft charging control" and for environmental plasma diagnoses. The present paper suggests instead thermal, field emitters of lanthanum (or perhaps cerium) hexaboride (LaB_6) with temperature variability up to ~ 1500K. Such emitters operate at much lower voltages with considerably more control and add plasma-diagnostic versatility. These gains should outweigh the additional complexity of providing heat for the LaB_6 thermal, field emitter.

THE CONCEPT OF SPACECRAFT-CHARGING CONTROL WITH FIELD EMISSION

Field-emission control of negative spacecraft charging in energetic plasmas is a concept discussed in references 1 and 2. Left uncontrolled, superficial potentials often build to several kilovolts when photo- and secondary-emissive effects fail to counteract the collection of high-energy electrons (refs. 1 to 5). This condition occurs on eclipsed spacecraft or shadowed, insulated surfaces. And charge accumulation could arise near Jupiter where photoemission is one and a half orders of magnitude lower than that in the orbit of the earth (ref. 1). Such effects complicate spacecraft operations and environmental measurements (ref. 6).

Solutions to spacecraft-charging problems include thermionic and plasma ejections of collected energetic electrons (ref. 5) as well as field emission, which also allows plasma diagnoses (refs. 1 and 2). References 1 and 2 logically propose cold tungsten (W) field emitters as simple, economical control devices. But good reasons also exist for using lanthanum-hexaboride (LaB_6) field emitters with moderate heating capabilities. This paper presents some advantages of the latter arrangement as a contribution to enable enlightened selection of a method for controlling spacecraft charging.

The present report advocates field emitters of 310,100, and/or 110 LaB_6 ($\phi_{LaB_6} \approx 2.5$ eV) (refs. 7 to 12) rather than W ($\phi_W \approx 4.5$ eV). Probe points with radii of curvature smaller than 10^{-5} cm are readily attainable (private communication with L. W. Swanson). So such dimensions in conjunction with up to several kilovolts between the spacecraft and its environment determine local electric fields in appropriate configurations. Also considered are field-emitter thermal variations up to ~ 1500K. Such variability should allow much greater operating ranges and flexibilities than cold W field emitters to justify the increased complication.

TECHNICAL ASPECTS OF THERMAL, FIELD EMISSION FOR SPACECRAFT-CHARGING CONTROL

Thermal, field emission brings an additional degree of freedom to the concept of spacecraft-charging control advanced in references 1 and 2: Now thermionic emission adds to field emission. And although this gain may be unimportant for a field emitter operating at 10^8 V/cm, it can be critical at $10^{6.5}$ V/cm.

These extremes as well as the middle ground appear in figures 1 to 8: Figures 1 to 4 comprise trends of emission current densities and of cooling voltages taken from reference 13. And figures 5 to 8 are working versions plotted from reference 14 data. The results derive from an image potential terminated at the emitter Fermi level as in the figures on page 7 of reference 15, page 275 of reference 16, and page 3 of reference 17. Field-emission studies often rely on the Fowler, Nordheim solution or its thermal modification (ref. 18)--both based on the nonterminated image potential (NIP). But all the previously mentioned figures represent the terminated image potential (TIP) modeled, mathematically described, discussed, and compared in reference 19 (and in the Appendix, for the reader's convenience). The TIP is relatively complicated and yields more conservative emission current densities than the NIP, particularly at very high electric fields.

But what electric fields (F_0) are probable in the spacecraft charging problem? Estimates are possible using the charging potentials (V) (several kilovolts), the radius of curvature for the field-emitter point (r) (10^{-5} cm), and an equation from reference 19:

$$F_0 = \alpha F_{sph} + (1-\alpha) F_{hyp} = V\left(\frac{\alpha}{r} + \frac{2(1-\alpha)}{r \log \frac{4R}{r}}\right) \qquad (1)$$

The total field comprises contributions from spheroid-like (F_{sph}) and hyperboloid-like (F_{hyp}) tip-shape effects. However, if the

field-emitter point is predominantly hyperboloid, as is often the case, the shape factor α is zero:

$$F_o \approx \frac{2V}{r\log\frac{4\ell}{r}} \approx \frac{10^5 V}{3} \text{ (for } l=2.5 \text{ cm)} \approx \frac{10^5 V}{4} \text{ (for } l=2.5 \text{ m)} \approx \frac{10^5 V}{5} \text{ (for } l=0.25 \text{ km)}$$
$$\approx \frac{10^5 V}{6} \text{ (for } l=25 \text{ km)} \approx \frac{10^5 V}{7} \text{ (for } l=2500 \text{ km)} \qquad 2)$$

Here ℓ is the distance from the field emitter to the effective anode. So for representative spacecraft-charging calculations using a hyperboloid emitter point with a 10^{-5} cm radius of curvature, a good field approximation is possible:

$$F_o \approx 0.2V \times 10^5 \text{ V/cm} \qquad 3)$$

Thus, spacecraft charging to several kilovolts (refs. 1 to 5) is equivalent to ~ 10^8 V/cm for field emission or about 6×10^7 A/cm^2 with a W field emitter (neglecting the limitations of the TIP theory). But even a high-melting, well-conducting W point requires microsecond pulsing not faster than ~ 1000 sec^{-1} to avoid destruction at such current densities (ref. 15). For continuous operation ~ 10^5 A/cm^2 is desirable. However, $10^{7.5}$ V/cm (~ 1.6 kilovolts) reduces emission to ~ 20 A/cm^2. And 10^7 V/cm or about 500 volts results in ~ 10^{-17} A/cm^2 for a cold W field emitter. So additional degrees of freedom seem desirable to allow spacecraft-charging reduction at lower voltages and with more than rather-precipitous control.

With 10^7 V/cm LaB_6 field emitters produce ~ 0.1 A/cm^2 cold, ~ 70 A/cm^2 at 1000K, and ~ 10^4 A/cm^2 at 1500K. Using 1500K LaB_6 field emitters yields ~ 100 A/cm^2 at $10^{6.5}$ V/cm or about 160 volts of spacecraft charging. In fact 1500K LaB_6 emits ~ 1 A/cm^2 with effectively no electric field. Of course, in the absence of space-charge neutralization by plasma ions, some small voltage is desirable to maintain a zero or slight electron-accelerating field. This condition allows unhindered thermionic or even Schottky emission (Appendix: page 6). W requires ~ 2550K to emit ~ 1 A/cm^2. And LaB_6 field emitters maintain their points more effectively than their tungsten counterparts at temperatures well above 1500K and at great electric fields (private communication with L. Swanson).

Cerium hexaboride (CeB_6) has slightly higher vapor pressures but somewhat lower work functions than LaB_6 (actually $LaB_{6.01}$ to $LaB_{6.1}$ refs. 7 to 10, 20, 21). So CeB_6 thermal field emitters should also prove to be good candidates for spacecraft-charging control.

ADVANTAGES OF SPACECRAFT-CHARGING CONTROL WITH LaB_6 THERMAL, FIELD EMITTERS

Reference 1 advocates a probe with cold W field emitters for "spacecraft charging control" and for environmental plasma diagnoses.

The present paper recommends instead thermal, field emitters of LaB_6 (or perhaps CeB_6) with temperature variability up to ~ 1500K. The LaB_6 thermal, field emitters relieve spacecraft charging at much lower voltages with considerably more control. These advantages come at the cost of additional complexity in providing heat for the LaB_6 thermal, field emitters. But such heating practices are common in laboratory studies of thermal, field emission. The LaB_6 thermal, field emitter also adds versatility to the plasma-diagnostic capabilities of the probe. So the choice is one of sacrificing some simplicity for greater operating range, flexibility, and control.

REFERENCES

1. Grard, Réjean J. L.: Spacecraft Charging Control by Field Emission. J. Geophys. Res., vol. 81, no. 10, Apr. 1, 1976, pp. 1805-1806.

2. Grard, R.: Spacecraft Potential Control and Plasma Diagnostic Using Electron Field Emission Probes. Space Sci. Instrum., vol. 1, Aug. 1975, pp. 363-376.

3. DeForest, S. E.: Spacecraft Charging at Synchronous Orbit. J. Geophys. Res., vol. 77, no. 4, Feb. 1, 1972, pp. 651-659.

4. DeForest, S. E.: Electrostatic Potentials Developed by ATS-5. Photon and Particle Interactions with Surfaces in Space, R. Grard, ed., D. Reidel (Dordrecht, Netherlands), 1973, pp. 263-276.

5. Bartlett, R. O.; DeForest, S. E.; and Goldstein, R.: Spacecraft Charging Control Demonstration at Geosynchronous Altitude. AIAA Paper 75-359, Mar. 1975.

6. Fredricks, R. W. and Scarf, F. I.: Observations of Spacecraft Charging Effects in Energetic Plasma Regions. Photon and Particle Interactions with Surfaces in Space, R. Grard, ed., D. Reidel (Dordrecht, Netherlands), 1973, pp. 277-308.

7. Swanson, L. W.; Dickinson, J. T.; and McNeely, D. R.: Fabrication and Surface Characterization of Composite Refractory Compounds Suitable for Thermionic Converters. NASA CR-2668, 1976.

8. Swanson, L. W.; Gresley, M.; and McNeely, D. R.: Fabrication and Surface Characterization of Composite Refractory Compounds Suitable for Thermionic Converters. (Interim Report #2, Oregon Graduate Center; NASA Grant NSG-3054.) NASA CR-135374, 1977.

9. Swanson, L. W.; Gresley, M.; and McNeely, D. R.: Fabrication and Surface Characterization of Composite Refractory Compounds Suitable for Thermionic Converters. (Interim Report #3, Oregon Graduate Center; NASA Grant NSG-3054.) NASA CR-135375, 1977.

10. Swanson, L. W. and McNeely, D. R.: Surface Characterization and Electron Emission Characteristics of BaB_6, LaB_6, CeB_6, and SmB_6. Presented at the World Electrotechnical Congress (Moscow, USSR), June 21-25, 1977.

11. Morris, J. F.: The NASA Thermionic-Conversion (TEC-ART) Program. IEEE Trans. Plasma Sci., vol. PS-6, no. 2, June 1978, pp. 180-190.

12. Morris, James F.: High-Efficiency, Low-Temperature Cesium Diodes with Lanthanum-Hexaboride Electrodes. NASA TM X-71549, 1974.

13. Morris, James F.: Energy Transport by Thermal Field Emission. NASA TN D-3448, 1966.

14. Morris, James F.: Calculations of Thermal, Field Emission for a Terminated Image Potential. NASA SP-3023, 1966.

15. Gomer, Robert: Field Emission and Field Ionization. Harvard University Press, 1961.

16. Conway, B. E.: Theory and Principles of Electrode Processes. The Ronald Press Co., 1965.

17. Morris, James F.: Thermal, Field Emission with a Terminated Image Potential. NASA TN D-2784, 1965.

18. Dyke, W. P. and Dolan, W. W.: Field Emission. Advances in Electronics and Electron Physics, Vol. 8, L. Marton, ed., Academic Press, Inc., 1956, pp. 90-.85.

19. Good, R. H., Jr.; and Müller, E. W.: Field Emission. Handbuck der Physik, vol. 21: Electron-Emission Gas Discharges I, S. Flügge, ed., Springer-Verlag (Berlin), 1956, pp. 176-231.

20. Jacobson, D. L. and Storms, E. K.: Work Function Measurement of Lanthanum Boron Compounds. IEEE Trans. Plasma Sci., vol. PS-6, no. 1, June 1978, pp. 191-199.

21. Storms, Edmund and Mueller, Barbara: Phase Relationship, Vaporization, and Thermodynamic Properties of the Lanthanum-Boron System. J. Phys. Chem., vol. 82, no. 1, 1978, pp. 51-59.

APPENDIX: NASA TN D-2784, April 1965

THERMAL, FIELD EMISSION WITH A TERMINATED IMAGE POTENTIAL

by James F. Morris

Lewis Research Center

SUMMARY

This paper develops a theory for thermal, field emission with an image potential that terminates at the emitter Fermi level. The resulting equations predict currents over and through the confining potential barrier. In addition, penetration probabilities and their generating functions are tabulated for fields from 10^5 to 10^9 volts per centimeter and for all emitter Fermi levels and work functions. Results are compared with those obtained for the nonterminated image potential.

INTRODUCTION

Interest in the effects of high electric fields on electron emission increases steadily. This growing importance of thermal, field emission is the result of better products. Many electronic devices improve, and new ones evolve with the accelerating utilization of dense currents from intense fields. Furthermore, the use of thermal, field emission in instrumentation and microscopy expands continuously. Therefore, there is a need to understand better the mechanism of electron emission, and this theoretic work aims at that goal.

Electron emission increases in two ways when the electric field applied to the emitter rises. The field reduces both the height and the width of the potential barrier that confines the electrons; thus, more current passes over and through the diminished barrier. Both suprabarrier and intrabarrier emission processes are examined in the present study.

The electron escape rate at high fields depends strongly on the value at which the freespace potential ends on the emitter face. For this reason, most theoretic approaches to thermal, field emission began with some type of terminated image potential, but for simplicity, the ordinary (nonterminated) image potential was used in the derivations. In this work, an image potential that joins the surface at the Fermi level is used throughout. Because a surface potential higher than the Fermi level is difficult to justify, thermal, field emission theories for the nonterminated image potential (NIP) and this terminated version (TIP) probably bracket reality.

The present paper presents approximations for suprabarrier emission (Richardson-Dushman, Schottky, and zero- and first-order TIP). Intrabarrier emission is indicated by a tabulation of penetration probabilities for fields from 10^5 to 10^9 volts per centimeter and for all emitter Fermi levels and work functions. With these transmission coefficients, the electron supply function, and the suprabarrier emission equation, the total thermal, field emission current can be estimated.

THEORY

The object of this quest is the prediction of suprabarrier and intrabarrier thermal-field emission for an image potential that terminates at the Fermi level on the emitter face.

TIP Barrier

Traditionally, the simple image potential connects with some arbitrary curvature to the bottom of the conduction band at the surface of the emitter (ref. 1). This alters the potential barrier slightly from that for the nonterminated image except at high field intensities. Therefore, the complications of the terminated image potential yielded to the simplicity of the ordinary image in most developments. At moderate fields, this is an appropriate approximation, but what are the high-field effects of a TIP?

In picking the point of potential termination, superficial conditions must be considered. Because surface atoms cannot satisfy their electron needs by lattice continuation, they attract electrons and unbalance the local charge. Furthermore, space-charge equilibrated emission hangs a compact cloud of electrons about emitter boundaries; thus, the electron potential rises sharply at the face of the metal.

A near-equilibrium condition must prevail for any simple emission theory to apply. In this model, the Fermi level remains constant throughout the metal, and the great number of electrons near the Fermi level satisfies the need for excess surface electrons with negligible depletion of the bulk distribution. Therefore, it appears that the electron potential might approach but not exceed the Fermi level at the surface of a pure metal.

For this reason, an image potential that ends at the Fermi level on the emitter face was chosen as the other limit of a range of simple theories for thermal, field emission that begins with the ordinary image.

Because the path between the superficial and internal emitter electron potentials is unknown, the present model sides with simplicity and drops from the Fermi level to

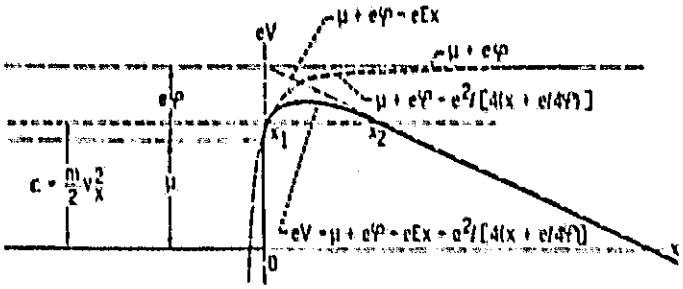

Figure 1. - Energy diagram for TIP electron emission.

the bottom of the conduction band on the surface. This vertical wall and its crowning corner create questions of electron reflections at abrupt potential changes. The wall and corners of the TIP model, however, are mere approximations of a rapidly but smoothly changing potential; they have no physical significance. Furthermore, the ordinary image potential approaches verticality near the emitter surface. So in line with previous field-emission theory, high rates of potential change, where electrons are reflected, are neglected.

Figure 1 diagrams the barrier formed when the potentials for a freespace electron and for the metal connect at the emitter surface (Symbols are defined in the appendix). Propst (ref. 2) used this type of TIP to predict the energy distribution of electrons ejected from tungsten by low-energy helium ions (He^{+}).

The terminated image potential (TIP = $-e^2/(4x + e/\varphi)$) results from shifting the ordinary image (NIP = $-e^2/4x$) to intercept the emitter face at the Fermi level; this is an 0.8-angstrom move for a 4.5-volt work function.

TIP Suprabarrier Emission

The TIP barrier

$$eV = \mu + e\varphi - eEx - \frac{e^2}{4\left(x + \frac{e}{4\varphi}\right)} \tag{1}$$

maximizes at

$$x_{max} = \frac{e}{2(eE)^{1/2}} - \frac{e}{4\varphi} \tag{2}$$

with a value of

$$eV_{max} = \mu + e\varphi - (e^3E)^{1/2} + \frac{e^2E}{4\varphi} \tag{3}$$

for fields up to $\epsilon^2 \times 10^8/3.6$ volts per centimeter; higher fields maintain the maximum potential at the Fermi level on the emitter surface.

Of course, in the NIP case,

$$x_{max} = \frac{e}{2(eE)^{1/2}}$$

and

$$eV_{max} = \mu + e\phi = (e^3E)^{1/2}$$

The potential maximum equals the minimum kinetic energy (based on the outwardly directed velocity component) that an internal electron requires to escape the emitter in simple suprabarrier emission theory.

These outgoing electrons within the metal distribute in the following manner (ref. 3):

$$n(v_x)dv_x = m\,dv_x \int_{-\infty}^{\infty}\int_{-\infty}^{\infty} n(p)dp_y\,dp_z$$

$$= \frac{4\pi m^2 kT}{h^3} m dv_x \int_0^{\infty} \frac{e^{-\left\{\left[\left(p_{yz}^2+p_x^2\right)/2m\right]-\mu\right\}/kT} p_{yz}\,dp_{yz}}{mkT\left(1+e^{-\left\{\left[\left(p_{yz}^2+p_x^2\right)/2m\right]-\mu\right\}/kT}\right)}$$

$$= \frac{4\pi m^2 kT}{h^3} \ln\left\{1+e^{\left[\mu-(m/2)v_x^2\right]/kT}\right\} dv_x \qquad (4)$$

This distribution, integrated from the potential barrier maximum to infinity, yields the equation for suprabarrier emission:

$$J_{TIP} = \frac{4\pi m^2 \kappa T e}{h^3} \int_{(2eV_{max}/m)^{1/2}}^{\infty} \ln\left\{1 + e^{-\left[(m/2)v_x^2 - \mu\right]/\kappa T}\right\} \frac{\kappa T}{m} \frac{m v_x \, dv_x}{\kappa T}$$

$$= \frac{4\pi m(\kappa T)^2 e}{h^3} \int_{\infty}^{eV_{max}} \ln\left[1 + e^{-(\epsilon - \mu)/\kappa T}\right] \left(-\frac{d\epsilon}{\kappa T}\right)$$

$$= \frac{4\pi m(\kappa T)^2 e}{h^3} \left\{ e^{\left[e\varphi - (e^3E)^{1/2} + (e^2E/4\varphi)\right]/\kappa T} - \frac{e^{-2\left[e\varphi - (e^3E)^{1/2} + (e^2E/4\varphi)\right]/\kappa T}}{4} \right.$$

$$\left. + \frac{e^{-3\left[e\varphi - (e^3E)^{1/2} + (e^2E/4\varphi)\right]/\kappa T}}{9} - \frac{e^{-4\left[e\varphi - (e^3E)^{1/2} + (e^2E/4\varphi)\right]/\kappa T}}{16} + \cdots \right\} \quad (5)$$

The zero order approximation is the TIP version of the Schottky equation.

Approximation for Suprabarrier Emission

Two suprabarrier emission equations compare clearly as the log of the ratio of their current densities for a given set of conditions. This approach eliminates debates about effective areas and coefficients ($120T^2$) and reduces the comparison to the difference of two exponents. An electric-field effect might then be considered significant when the current-density ratio for the two emission equations reaches 1.001 or 0.999. This is the comparative criterion in the following evaluations for T in ^{o}K, φ in volts, and E in volts per centimeter.

With these stipulations, little effort is required to isolate the areas of apparent applicability of Richardson Dushman (RD), Schottky (S), and zero- (TIP-0) and first-order (TIP-1) TIP approximations for suprabarrier electron emission.

In the following comparisons, the particular emission equation appears immediately after its name and is attended by the electric field at which its current density

differs by 0.1 percent from that of the next more complicated emission expression; of course, if the field were increased, the difference would be greater:

Richardson-Dushman:

$$J_{RD} = 120T^2 \exp\left(-\frac{e\phi}{\kappa T}\right)$$

$$\frac{J_{RD}}{J_S} = 0.999 \quad \text{at} \quad E = 5.16T^2 \times 10^{-8}$$

Schottky (NTP):

$$J_S = 120T^2 \exp\left[-\frac{e\phi - (e^3E)^{1/2}}{\kappa T}\right]$$

$$\frac{J_S}{J_{TTP-0}} = 1.001 \quad \text{at} \quad E = 2.4\phi T$$

Zero-order TTP:

$$J_{TTP-0} = 120T^2 \exp\left[-\frac{e\phi - (e^3E)^{1/2} + e^2E}{\kappa T}\right]$$

$$\frac{J_{TTP-0}}{J_{TTP-1}} = 1.001 \quad \text{at} \quad E = 0.278\phi^2\left[1 + 2.18\left(\frac{T}{\phi}\right)^{1/2} \times 10^{-2}\right]^2 \times 10^8$$

First-order TTP:

$$J_{TTP-1} = 120T^2\left\{e^{-\left[e\phi-(e^3E)^{1/2}+(e^2E/4\phi)\right]/\kappa T} - \frac{e^{-2\left[e\phi-(e^3E)^{1/2}+(e^2E/4\phi)\right]/\kappa T}}{4}\right\}$$

Both the TTP and NTP equations raise questions when fields rise to near 10^7 volts per centimeter. At this value, the potential maxima for these two models lie between

5 and 6 angstroms from the emitter surface. Because this is near the atomic dimension, the assumptions of the TIP and NIP models approximate the actual physical situation poorly.

TIP Tunneling

The kinetic energy of a tunneling electron is negative, and therefore, its momentum is imaginary. So within the emission barrier, an electron lies less likely at $x + \Delta x$ than at x. In accordance with the probability-density ratio for the two locations:

$$P = \frac{\psi^*(x+\Delta x)\psi(x+\Delta x)}{\psi^*(x)\psi(x)} = \frac{\exp\left[-2|k|(x+\Delta x)\right]}{\exp(-2|k|x)} = \exp(-2|k|\Delta x)$$

$$= \exp\left\{-\frac{2}{\hbar}\left[2m(eV-\epsilon)\right]^{1/2}\Delta x\right\} \qquad (6)$$

The product of such successive probability ratios through a barrier for a particular electron indicates the odds for escape by tunneling. This product of incremental probability ratios merely requires a summation of the exponents; thus, in the limit

$$P = \exp\left\{-\frac{2}{\hbar}\int_{x_1}^{x_2}\left[2m(eV-\epsilon)\right]^{1/2}dx\right\}$$

$$= \exp\left\{-\frac{2}{\hbar}\int_{x_1}^{x_2}\left[2m\left(\mu+e\varphi-eEx-\frac{e^2}{4x+\frac{e}{\varphi}}-\epsilon\right)\right]^{1/2}dx\right\} \qquad (7)$$

which is an approximation of the WKB result (ref. 1),

$$P = f(\epsilon, V)\exp\left\{-\frac{2}{\hbar}\int_{x_1}^{x_2}\left[2m(eV-\epsilon)\right]^{1/2}dx\right\} \approx \exp\left\{-\frac{2}{\hbar}\int_{x_1}^{x_2}\left[2m(eV-\epsilon)\right]^{1/2}dx\right\} \qquad (8)$$

where x_1 and x_2 are the turning points ($\epsilon = eV$) for the barrier (fig. 1).

Consequently, the penetration theory for the TIP emission barrier begins with the assumptions and restrictions of the WKB theory, and that leaves little but the actual integration and evaluation of the transmission coefficient (eq. (7)):

$$P \approx \exp\left[-\left(\frac{8^3 m}{h^2}\right)^{1/2} \int_{x_1}^{x_2} \left(\mu + e\varphi - eEx - \frac{e^3}{4x + e/\varphi} - \epsilon\right)^{1/3} dx\right]$$

$$= \exp\left\{-\frac{(2\beta)^{3/2} m^{1/2}}{heE} \int_{x_1}^{x_2} \left[1 + \frac{e^3 E}{4\beta^2 \varphi} - \frac{eE}{\beta}\left(x + \frac{e}{4\varphi}\right) - \frac{e^3 E}{4\beta^2 eE\left(x + \frac{e}{4\varphi}\right)}\right]^{1/3} \frac{eE\, dx}{\beta}\right\}$$

$$= \exp\left\{-\left(\frac{\alpha}{2}\right)^{-3/2}\left(\frac{\epsilon}{eE}\right)^{1/4} \int_{\eta_1}^{\eta_2} \left[1 + \left(\frac{\alpha}{2}\right)^3 \delta - \eta - \frac{(\alpha/2)^2}{\eta}\right]^{1/3} d\eta\right\} \tag{9}$$

At the turning points,

$$\frac{eV - \epsilon}{\beta} = 0 = 1 + \left(\frac{\alpha}{2}\right)^3 \delta - \eta - \frac{(\alpha/2)^2}{\eta} \tag{10}$$

Therefore,

$$\eta_{2,1} = \frac{1 + (\alpha/2)^2 \delta}{2}\left(1 \pm \left\{1 - \frac{4(\alpha/2)^3}{\left[1 + (\alpha/2)^2 \delta\right]^2}\right\}^{1/2}\right) \quad \text{for } \delta < 1 \tag{11}$$

When $\delta > 1$, however, the inner turning point is not η_1; instead, it is $(\alpha/2)^2\delta$ because $x_1 = 0$. Therefore, at this juncture a generalized inner turning point is defined as η_0, which is η_1 for $\delta < 1$ and $(\alpha/2)^2\delta$ for $\delta > 1$.

Now, as $\alpha \to 0$,

$$\int_{\eta_1}^{\eta_2} \left[1 + \left(\frac{\alpha}{2}\right)^2 \delta - \eta - \frac{(\alpha/2)^2}{\eta} \right]^{1/2} d\eta = \frac{2}{3} \tag{12}$$

Then, by definition,

$$I(\alpha, \delta) \equiv \frac{3}{2} \int_{\eta_1}^{\eta_2} \left[1 + \left(\frac{\alpha}{2}\right)^2 \delta - \eta - \frac{(\alpha/2)^2}{\eta} \right]^{1/2} d\eta \tag{13}$$

and

$$C(\alpha, E) \equiv \frac{2}{3} \left(\frac{\alpha}{2}\right)^{-3/2} \left(\frac{\xi}{eE}\right)^{1/4} \tag{14}$$

and the penetration probability (eq. (9)) becomes

$$P \approx \exp \left[- C(\alpha, E) I(\alpha, \delta) \right] \tag{15}$$

As $\delta \to 0$ with nonzero β,

$$I(\alpha, \delta) - I(\alpha) \equiv \frac{3}{2} \int_{\eta_1}^{\eta_2} \left[1 - \eta - \frac{(\alpha/2)^2}{\eta} \right]^{1/2} d\eta \tag{16}$$

and

$$\eta_{2,1} = \frac{1}{2} \left[1 \pm (1 - \alpha^2)^{1/2} \right] \tag{17}$$

These forms are identical with those for the nonterminated image potential, because as $\delta \to 0$, $\varphi \to \infty$ and causes TIP $\to$ NIP.

Both distances and potentials are real in the TIP model; consequently, α, β, δ, and η are all positive. Therefore, the number under the radical in equation (11) for $\eta_{2,1}$ must fall between zero and one.

$$0 \leq \frac{4(\alpha/2)^2}{\left[1 + (\alpha/2)^2\delta\right]^2} \leq 1 \tag{18}$$

This limits α for δ's between zero and one to

$$0 \leq \alpha \leq \frac{2\left[1 - (1-\delta)^{1/2}\right]}{\delta} \tag{19a}$$

and

$$\infty \geq \alpha \geq \frac{2\left[1 + (1-\delta)^{1/2}\right]}{\delta} \tag{19b}$$

Each range of α yields positive η_1's and η_2's; however, the higher range gives negative values of x. Thus, only the lower α range is physically meaningful; the upper limits for α in the TIP model are shown in table I.

For $\delta > 1$,

$$\frac{4(\alpha/2)^2}{\left[1 + (\alpha/2)^2\delta\right]^2}$$

cannot climb to unity regardless of the α value; thus, inequality (18) is satisfied.

Now equation (13) can be integrated.

$$I(\alpha,\delta) = \frac{3}{2}\int_{\eta_0}^{\eta_2}\left[1+\left(\frac{\alpha}{2}\right)^2\delta-\eta-\frac{(\alpha/2)^2}{\eta}\right]^{1/2}d\eta = 3\int_{\eta_0^{1/2}}^{\eta_2^{1/2}}\left[(\eta_2-\eta)(\eta-\eta_1)\right]^{1/2}d(\eta^{1/2}) = \frac{3(\eta_2-\eta_1)^2}{\eta_2^{1/2}}\int_0^{u_1} sn^2u\,cn^2u\,du$$

$$= \frac{(\eta_2-\eta_1)^2}{\eta^{1/2}K^4}\left[(2-K^2)E(u) - 2K^2u - K^2 sn\,u\,cn\,u\,dn\,u\right]_0^{u_1}$$

$$= \frac{(\eta_2-\eta_1)^2}{\eta_2^{1/2}\left(\frac{\eta_2-\eta_1}{\eta_2}\right)^2}\left[\left(2-\frac{\eta_2-\eta_1}{\eta_2}\right)E(u_1) - 2\left(1-\frac{\eta_2-\eta_1}{\eta_2}\right)u_1 - \frac{\eta_2-\eta_1}{\eta_2}\left(\frac{\eta_2-\eta_0}{\eta_2-\eta_1}\right)^{1/2}\left(1-\frac{\eta_2-\eta_0}{\eta_2-\eta_1}\right)^{1/2}\left(1-\frac{\eta_2-\eta_1}{\eta_2}\frac{\eta_2-\eta_0}{\eta_2-\eta_1}\right)^{1/2}\right]$$

$$= \eta_2^{1/2}(\eta_2+\eta_1)\left[E(u_1) - \frac{2\eta_1}{\eta_2+\eta_1}u_1 - \frac{(\eta_2-\eta_0)^{1/2}(\eta_0-\eta_1)^{1/2}\eta_0^{1/2}}{\eta_2^{1/2}(\eta_2+\eta_1)}\right]$$

$$= \left\{\left[1+\left(\frac{\alpha}{2}\right)^2\delta\right]^3\frac{1+\gamma}{2}\right\}^{1/2}\left[E(\Phi,K) - (1-\gamma)F(\Phi,K) - \left(\frac{\eta_0\left\{\left[1+\left(\frac{\alpha}{2}\right)^2\delta\right]\eta_0 - \eta_0^2 - \left(\frac{\alpha}{2}\right)^2\right\}}{\left[1+\left(\frac{\alpha}{2}\right)^2\delta\right]^3\frac{1+\gamma}{2}}\right)^{1/2}\right] \tag{20}$$

where

$$\gamma = \left\{1 - \frac{4(\alpha/2)^2}{\left[1+(\alpha/2)^2\delta\right]^2}\right\}^{1/2}$$

$$K = \left(\frac{2\gamma}{1+\gamma}\right)^{1/2}$$

and, of course, $F(\Phi,K)$ and $E(\Phi,K)$ are incomplete elliptic integrals of the first and second kinds, respectively.

Because $\eta_0 = \eta_1$ for $\delta < 1$ and $\eta_0 = (\alpha/2)^2\delta$ for $\delta \geq 1$, two solutions for $I(\alpha,\delta)$ result. For $\delta < 1$,

$$\Phi = \sin^{-1}\left(\frac{\eta_2-\eta_0}{\eta_2-\eta_1}\right)^{1/2} = \frac{\pi}{2} \tag{21}$$

and

$$I(\alpha, \delta) = \left\{\left[1 + \left(\frac{\alpha}{2}\right)^2 \delta\right]^3 \left(\frac{1+\gamma}{2}\right)\right\}^{1/2} \left\{E\left[\left(\frac{2\gamma}{1+\gamma}\right)^{1/2}\right] - (1-\gamma)\, F\left[\left(\frac{2\gamma}{1+\gamma}\right)^{1/2}\right]\right\} \tag{22}$$

where $F(K)$ and $E(K)$ are complete elliptic integrals of the first and second kinds, respectively. For $\delta \geq 1$,

$$\Phi = \sin^{-1}\left(\frac{\eta_2 - \eta_0}{\eta_2 - \eta_1}\right)^{1/2} = \sin^{-1}\left\{\frac{\frac{1+\gamma}{2} - \left(\frac{\alpha}{2}\right)^2 \delta \Big/ \left[1 + \left(\frac{\alpha}{2}\right)^2 \delta\right]}{\gamma}\right\}^{1/2} \tag{23}$$

and

$$I(\alpha, \delta) = \left\{\left[1 + \left(\frac{\alpha}{2}\right)^2 \delta\right]^3 \frac{1+\gamma}{2}\right\}^{1/2} \left[E\left(\sin^{-1}\left\{\frac{\frac{1+\gamma}{2} - \left(\frac{\alpha}{2}\right)^2 \delta \Big/ \left[1 + \left(\frac{\alpha}{2}\right)^2 \delta\right]}{\gamma}\right\}^{1/2}, \left(\frac{2\gamma}{1+\gamma}\right)^{1/2}\right)\right.$$

$$- (1-\gamma)\, F\left(\sin^{-1}\left\{\frac{\frac{1+\gamma}{2} - \left(\frac{\alpha}{2}\right)^2 \delta \Big/ \left[1 + \left(\frac{\alpha}{2}\right)^2 \delta\right]}{\gamma}\right\}^{1/2}, \left(\frac{2\gamma}{1+\gamma}\right)^{1/2}\right)$$

$$\left. - \left\{\frac{\delta \left(\frac{\alpha}{2}\right)^4 (\delta - 1)}{\left[1 + \left(\frac{\alpha}{2}\right)^2 \delta\right]^3 \frac{1+\gamma}{2}}\right\}^{1/2}\right] \tag{24}$$

Values of $C(\alpha, E)$, $I(\alpha, \delta)$, and P are given in tables II to IV. More P values can be computed with other permutations of the tabulated C and I results.

These penetration probabilities can be used with the distribution function for outgoing electrons (eq. (4)) to predict tunneling currents for the TIP emission barrier.

The ranges of parameters for which C, I, and P are tabulated are extreme; certain of these parametric combinations produce conditions that preclude simple emission-barrier models or that cannot be realized physically. Therefore, the limitations of thermal, field emission theory should be checked before the results are applied.

Limitations of Thermal, Field Emission Theories

First, the effects of the TIP on thermal, field emission can be observed. TIP suprabarrier emission was compared with the Schottky (NIP) equation in an earlier section (Approximations for Suprabarrier Emission). The previous section and tables II to IV examine the NIP and TIP penetration probabilities; values for $\delta = 0$ are identical with NIP transmission coefficients (ref. 4). The differences between NIP and TIP theories are therefore obvious.

Neither the NIP nor the TIP barrier model stands under certain extreme conditions. For example, when the distance from the emitter face to the outside of the barrier reduces to near-atomic dimensions, the assumption of a smooth metal surface fails. Furthermore, if the emission density becomes a significant fraction of the internal electron density, the near-equilibrium assumption fails, and the Fermi-Dirac distribution cannot be used. Since these are high-field symptoms, both the NIP and TIP theories decrease in applicability as the electric field increases.

In addition to these simple problems, penetration difficulties must be considered. It was noted earlier that reflections caused by abrupt potential changes are not considered in the NIP and TIP models. It was also mentioned that the WKB restrictions apply; these requirements reside in the expression

$$\left|\frac{d\lambda}{dx}\right| = \left|\frac{h}{p^2}\frac{dp}{dx}\right| \ll 1 \tag{25}$$

which is the condition for negligible reflection of an electron wave. Obviously, then, the WKB approximation falters when $p \to 0$; this condition occurs near the turning points and near the maximum of the emission barrier. Electrons, however, that have a finite p as they pass under the barrier maximum adhere to WKB principles exactly, because $dp/dx = 0$ there. But the electron momentum function must satisfy equation (25) throughout much of the integration for $I(\alpha, \delta)$ for a good approximation.

Then there is the function $f(\epsilon, V)$ that multiplies the exponential in the complete WKB penetration probability (eq. (8)). The need for this function is debatable, and in any event, it causes differences of less than a factor of two in transmission coefficients at pertinent energy levels (ref. 5). If this refinement is deemed necessary, however, the present penetration probabilities can be multiplied by some apparently appropriate $f(\epsilon, V)$.

Finally, when all of these conditions have been properly met, the TIP results can be used to approximate thermal, field emission.

Lewis Research Center,
National Aeronautics and Space Administration,
Cleveland, Ohio, January 21, 1965.

APPENDIX - SYMBOLS

$C(\alpha, E)$	coefficient in exponent of penetration probability
E	electrostatic field, V/cm
E(K)	complete elliptic integral of second kind
$E(\Phi, K)$	incomplete elliptic integral of second kind
e	electronic charge
F(K)	complete elliptic integral of the first kind
$F(\Phi, K)$	incomplete elliptic integral of the first kind
f	function
h	Planck's constant
$\hbar$	Planck's constant divided by 2π
$I(\alpha, \delta)$	integral in exponent of penetration probability
i	imaginary
j	current density, A/sq cm
k	wave number for electron wave
K	modulus of elliptic integral
m	electronic mass
NIP	$-e^2/4x$, also refers to emission model using oridinary image potential
n(p)	electron number density in phase space
$n(v_x)$	electron number density dimensional and x-directed velocity space
P	penetration probability
p	electronic momentum
T	absolute temperature, ^{o}K
TIP	$-e^2/(4x + e/\varphi)$, also refers to emission model using image potential that terminates at Fermi level on emitter surface
V	potential
v	velocity
x	dimension normal to emitter surface
y	dimension in emitter surface
z	dimension normal to x and y
α	$e(eE)^{1/2}/\beta$
β	$\mu + e\varphi - \epsilon$
γ	$\left\{1 - 4(\alpha/2)^2/\left[1 + (\alpha/2)^2\delta\right]^2\right\}^{1/2}$
δ	$\beta/e\varphi$
ϵ	$mv_x^2/2$
η	$eE(x + e/4\varphi)/\beta$
κ	Boltzmann constant
λ	wavelength of electron wave
μ	Fermi level
ξ	$e^6m^2/\hbar^4$
Φ	upper limit of elliptic integral
φ	work function
Ψ	electronic wave function

ψ^*	complex conjugate of ψ

Subscripts:

max	maximum potential location
RD	Richardson-Dushman
S	Schottky
TIP	terminated image potential
TIP-0	TIP zero-order approximation
TIP-1	TIP first-order approximation
x, y, z	x, y, or z dimension
yz	y-z dimension space
0	generalized inside turning point on emission barrier
1	inner turning point above Fermi level on emission barrier
2	outer turning point on emission barrier

REFERENCES

1. Bohm, David: Quantum Theory. Prentice-Hall Inc., 1961.
2. Propst, F. M.: Energy Distribution of Electrons Ejected from Tungsten by He^+. Phys. Rev., vol. 129, no. 1, Jan. 1963, pp. 7-11.
3. Sommerfeld, A.; and Bethe, H.: Elektronentheorie der Metalle. Handbuch der Physik. Springer-Verlag (Berlin), vol. 24, pt. 2, 1933, pp. 333-622.
4. Burgess, R. E.; Kroemer, H.; and Houston, J. M.: Corrected Values of Fowler-Nordheim Field Emission Functions v(y) and s(y). Phys. Rev., vol. 90, no. 4, May 15, 1953, p. 515.
5. Dyke, W. P.; and Dolan, W. W.: Field Emission. Vol. VIII of Advances in Electronics and Electron Physics, L. Marton, ed., Academic Press, 1956, p. 93.

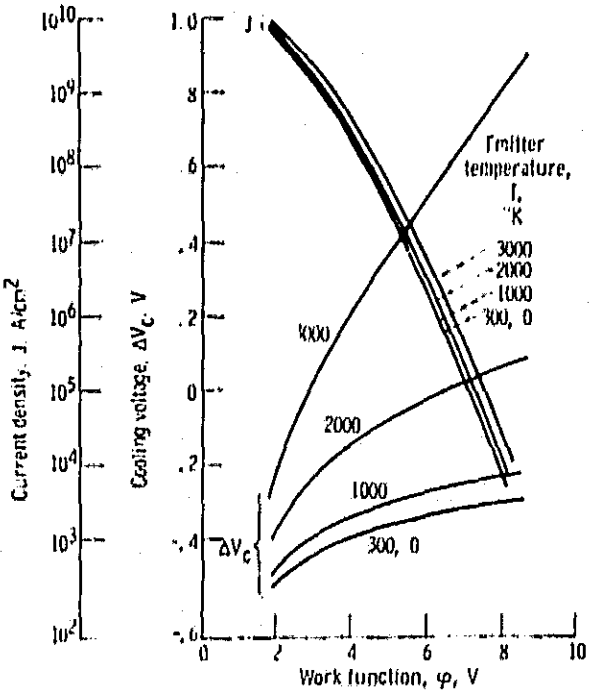

Figure 1. - Emitter cooling for 10^8 volts per centimeter. $\Delta Q_c = J\Delta V_c$.

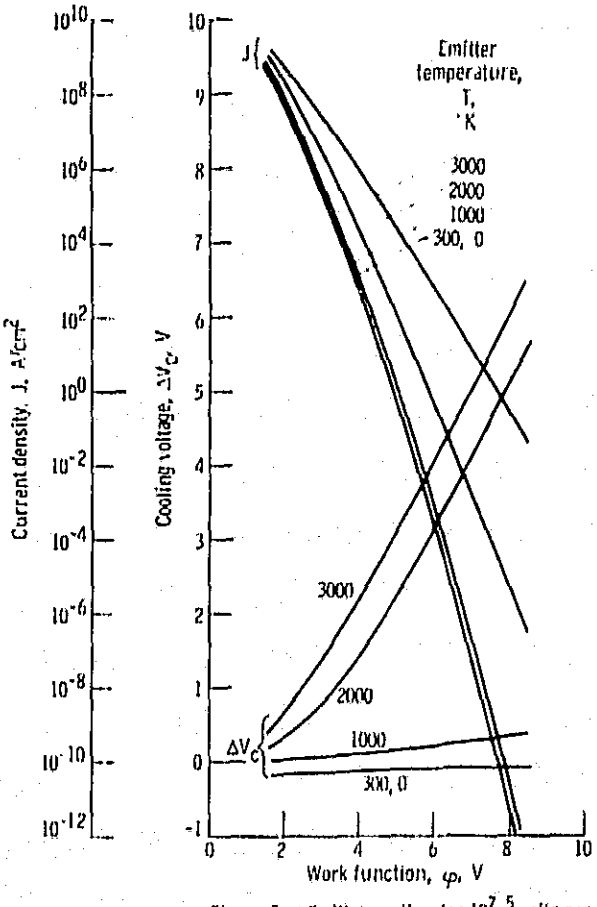

Figure 2. Emitter cooling for $10^{7.5}$ volts per centimeter. $\Delta Q_c = J\Delta V_c$.

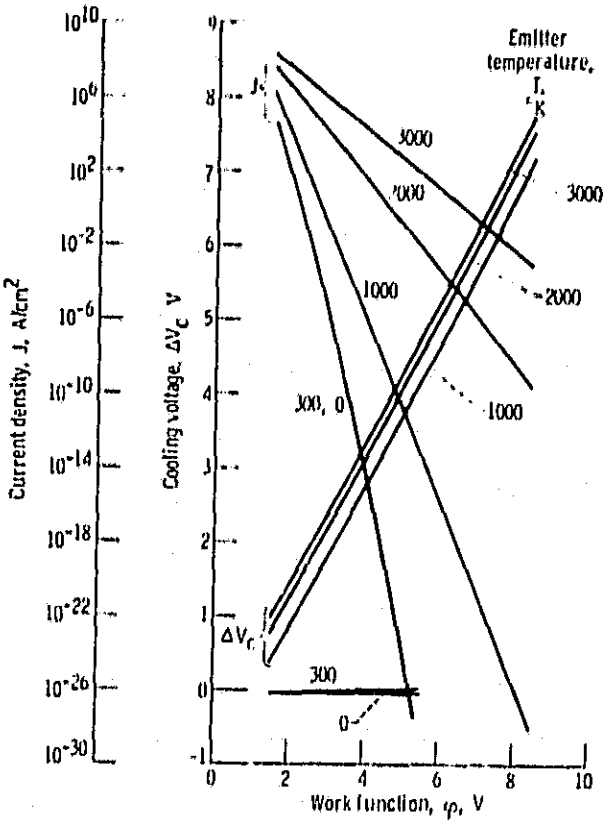

Figure 3. - Emitter cooling for 10^7 volts per centimeter. $\Delta Q_c = J\Delta V_c$.

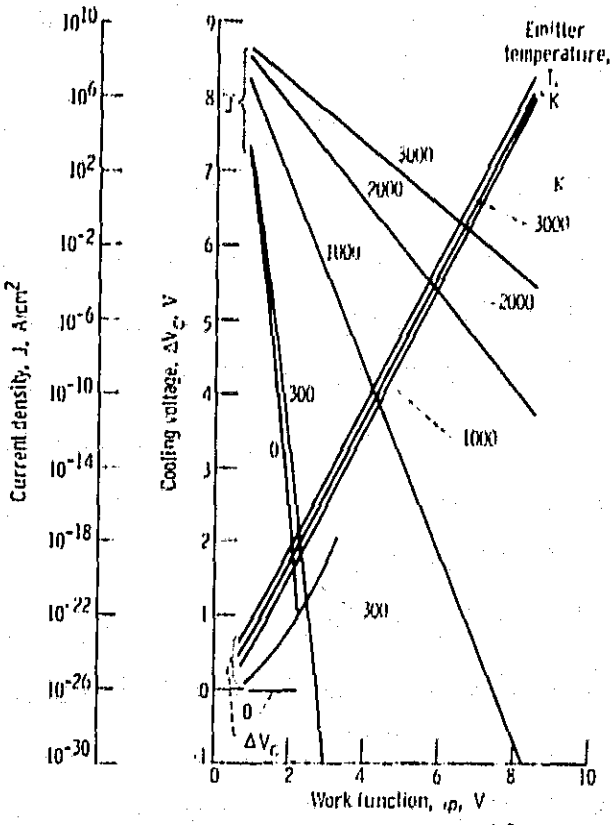

Figure 4. - Emitter cooling for $10^{6.5}$ volts per centimeter. $\Delta Q_c = J\Delta V_c$.

FIGURES 1 TO 4 (Ref. 13)

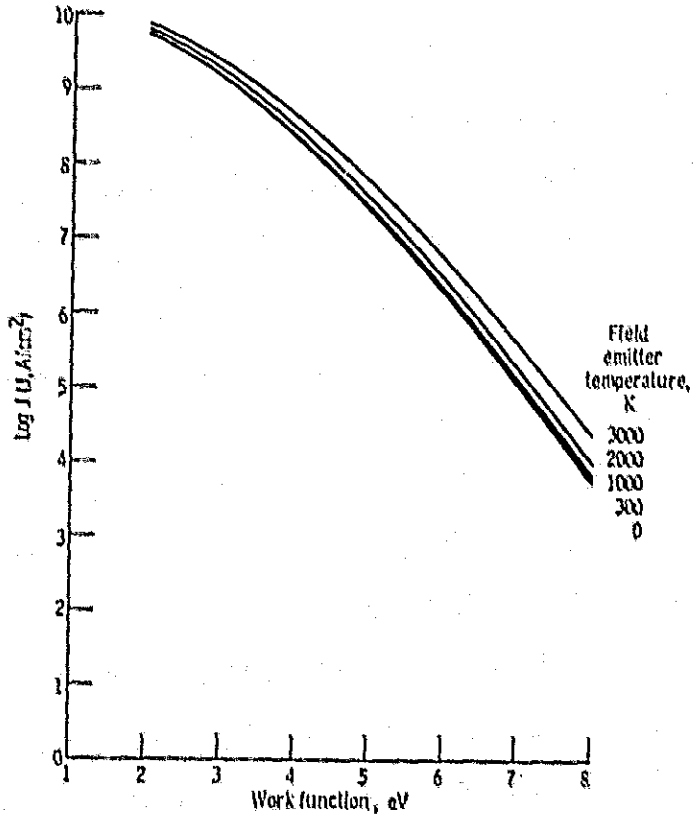

Figure 5. - Thermal, field emission with a terminated image potential; log (current density) vs. work function for a 10^8-V/cm electric field (ref. 14 data).

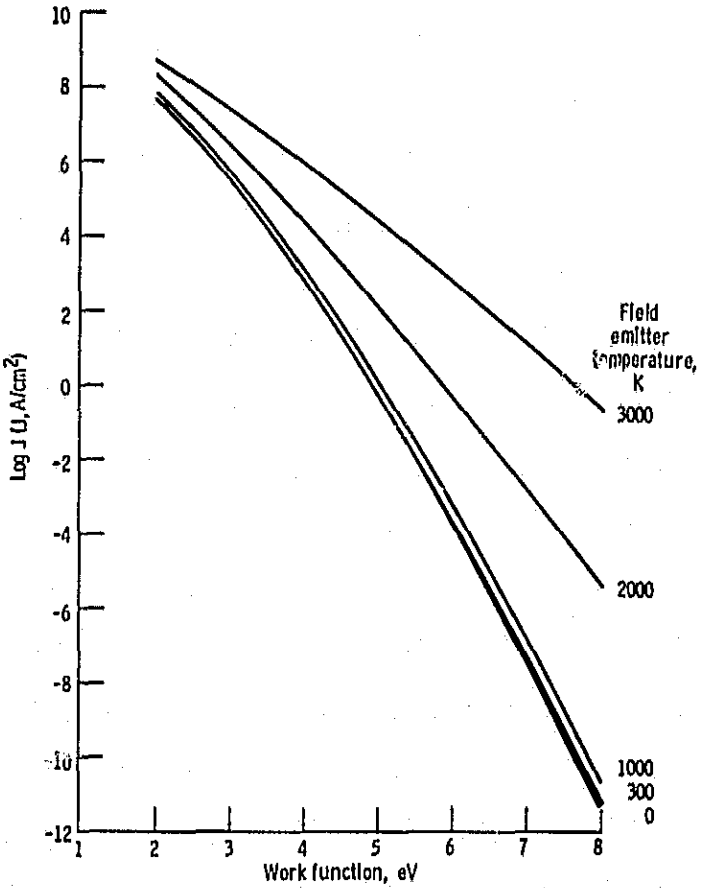

Figure 6. - Thermal, field emission with a terminated image potential; $\log_{10}$ (current density) vs. work function for a 10^7.5-V/cm electric field (ref. 14 data).

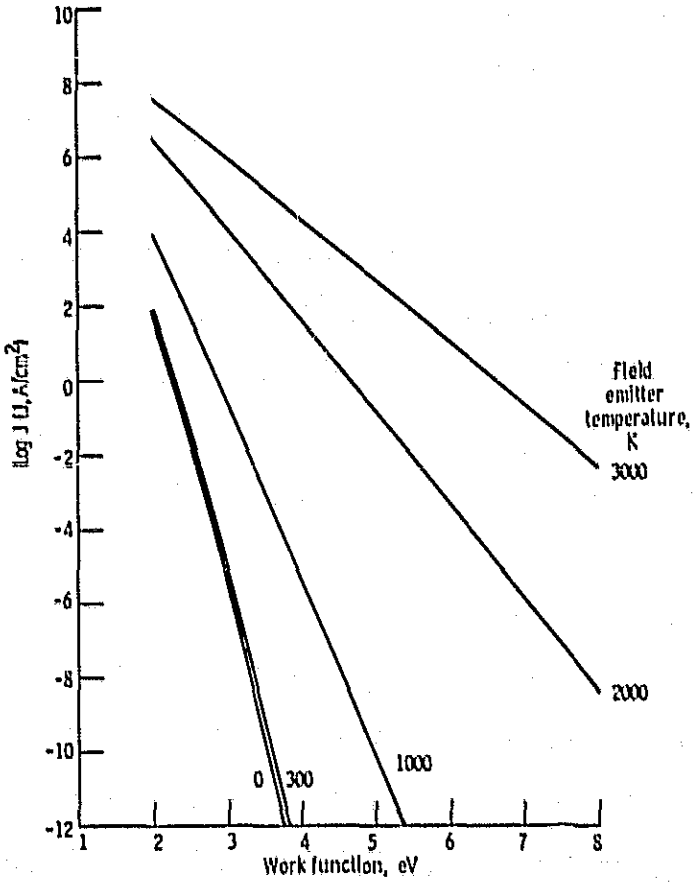

Figure 7. - Thermal, field emission with a terminated image potential; $\log_{10}$ (current density) vs. work function for a 10^7-V/cm electric field (ref. 14 data).

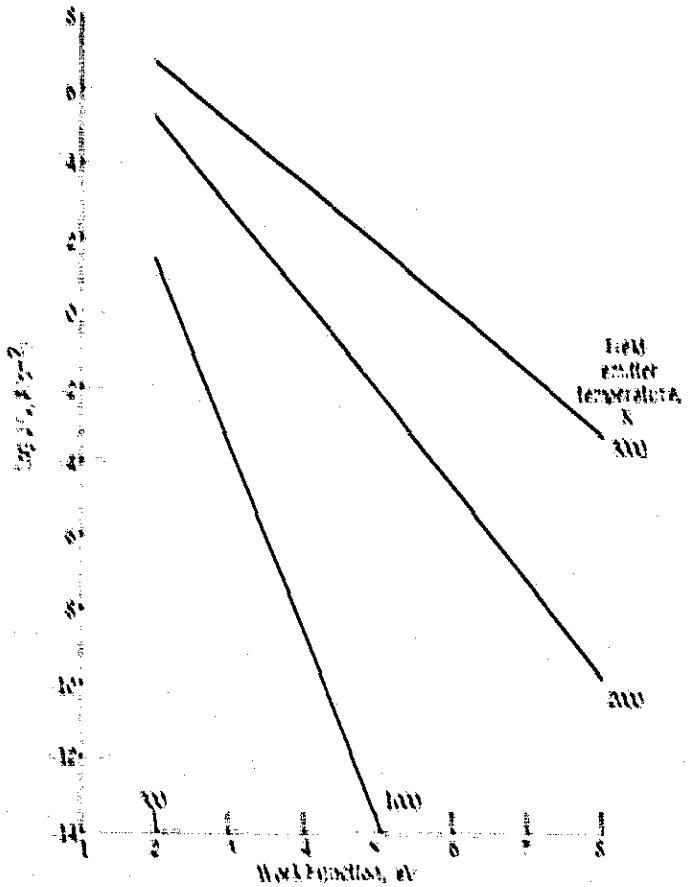

Figure 8. Thermal, field emission with a terminated image potential [illegible] current density vs. work function for a 10^{10} V/cm electric field (ref. 14 data).

1 Report No	2 Government Accession No	3 Recipient's Catalog No
NASA TM-78990		

4 Title and Subtitle	5 Report Date
SPACECRAFT CHARGING CONTROL BY THERMAL, FIELD EMISSION WITH LANTHANUM-HEXABORIDE EMITTERS	6 Performing Organization Code
7 Author(s) James F. Morris	8 Performing Organization Report No E-9773
9 Performing Organization Name and Address National Aeronautics and Space Administration Lewis Research Center Cleveland, Ohio 44135	10 Work Unit No 11 Contract or Grant No
12 Sponsoring Agency Name and Address National Aeronautics and Space Administration Washington, D.C. 20546	13 Type of Report and Period Covered Technical Memorandum 14 Sponsoring Agency Code

15 Supplementary Notes

16 Abstract

Recently R. Grard (J. Geophys. Rsch., V. 81, No. 10, p. 1805, April 1976) elaborated on his concept of using cold tungsten field emitters for "spacecraft charging control" and for environmental plasma diagnoses. The present paper suggests instead thermal, field emitters of lanthanum (or perhaps cerium) hexaboride (LaB_6) with temperature variability up to ~1500 K. Such emitters operate at much lower voltages with considerably more control and add plasma-diagnostic versatility. These gains should outweigh the additional complexity of providing heat for the LaB_6 thermal, field emitter.

17. Key Words (Suggested by Author(s))	18. Distribution Statement
Spacecraft charging; Spacecraft environmental diagnostics; Field emission; Thermal, field emission; Lanthanum hexaboride; Cerium hexaboride; Tungsten	Unclassified - unlimited STAR Category 88

19. Security Classif. (of this report)	20. Security Classif. (of this page)	21. No. of Pages	22. Price*
Unclassified	Unclassified		

* For sale by the National Technical Information Service, Springfield, Virginia 22161